Journal of Inorganic Biochemistry 134 (2014) 1–11

Contents lists available at ScienceDirect

Journal of Inorganic Biochemistry

journal homepage: www.elsevier.com/locate/jinorgbio

A ruthenium(II) complex capable of inducing and stabilizing bcl-2 G-quadruplex formation as a potential cancer inhibitor

Jingnan Zhang [a,1], Qianqian Yu [a,1], Qian Li [a], Licong Yang [a], Lanmei Chen [a,b], Yanhui Zhou [a,*], Jie Liu [a,*]

[a] Department of Chemistry, Jinan University, Guangzhou 510632, PR China
[b] School of Pharmacy, Guangdong Medical College, Zhanjiang, 524023, PR China

ARTICLE INFO

Article history:
Received 23 September 2013
Received in revised form 12 December 2013
Accepted 13 December 2013
Available online 24 December 2013

Keywords:
Ruthenium
Bcl-2
G-quadruplexes
DNA structures
Anticancer

ABSTRACT

Two ruthenium(II) complexes (Ru-complexes) were synthesized and characterized in this study. The selectivity and ability of the complexes to interact with bcl-2 DNA were investigated here. It turned out that $[Ru(ip)_3](ClO_4)_2 \cdot 2H_2O$ (complex 1, ip = 1H-iminazole [4,5-f][1,10] phenanthroline) could induce and stabilize the formations of G-quadruplexes more effectively than $[Ru(pip)_3](ClO_4)_2 \cdot 2H_2O$ (complex 2, pip = 2-phenylimidazo-[4,5-f][1,10]phenanthroline) did. Considering the important role of the Ru-complex ligand in inducing and stabilizing the formations of G-quadruplex in our previous studies, we speculate that the overlarge ligand of complex 2 may block its binding affinity for G-quadruplexes. Complex 1 also induced cell apoptosis in in vitro assays. In general, this study provided potentially important information for further development of the Ru-complexes as good inducers and stabilizers of bcl-2 G-quadruplex DNA for cancer treatment.

1. Introduction

G-quadruplexes found throughout the human genome are considered as potential anticancer targets. Many promoter regions could form G-quadruplex structures, resulting in gene regulation at the level of transcription. This suggestion has led to extensive investigations of the role of G-quadruplex formation in the transcriptional regulation of oncogenic promoters such as bcl-2 [1], c-myc [2], VEGF [3], HIF-1α [4], and c-kit [5,6].

The bcl-2 gene product is a mitochondrial membrane protein that has an essential function in cell survival; it exists in a delicate balance with other apoptosis-related proteins and functions as an inhibitor of cell apoptosis [7,8]. With its crucial role in apoptosis regulation, the bcl-2 gene is already viewed as an important target in anticancer treatment using pro-apoptotic drugs.

The human bcl-2 gene has two promoters, P1 and P2 [9], for controlling its transcriptional initiation. The P1 promoter, which is the principal transcriptional promoter for bcl-2 gene, is a GC-rich region capable of forming G-quadruplex [10]. The GC-rich region upstream of the P1 promoter has been shown to be critically involved in the regulation of bcl-2 gene expression, thereby controlling the occurrence of cancer diseases. Numerous studies have focused on understanding quadruplex-mediated alteration in the molecular recognition of the promoter regions, thus indicating their influence on disease phenotypes. The interactions between G-quadruplexes and small molecules have become interesting to study because of their formations, structures, and stabilities. Many ligands exhibiting structural recognition and high affinity for G-quadruplex DNA have been characterized for their ability to induce and stabilize G-quadruplexes. Most G-quadruplex binding ligands reported thus far have planar aromatic molecules, which are capable of inducing interaction with guanine tetrads via π–π interactions. In addition, they also have side chains directed toward the quadruplex loops [11–14]. However, the selectivity of these ligands for G-quadruplex DNA over duplex DNA is mostly poor, usually resulting in acute toxic and intolerable side effects on normal tissues. Hence, increased selectivity for G-quadruplex and low cytotoxicity are among the factors to consider in designing drugs targeting the bcl-2 G-quadruplex for cancer chemotherapy [15–17]. Only a few Ru-complexes have been currently verified to promote the formation and stabilization of G-quadruplexes [18]. Shi et al. have reported the remarkable ability of a novel dinuclear complex to promote antiparallel G-quadruplex formation [19]. Thomas and co-workers investigated the binding preferences of a dinuclear ruthenium(II) complex with different quadruplex DNA structures. They found that the differences in quadruplex binding affinity and optical signature are consequences of the structural features of the quadruplexes [20]. They also reported that the Ru-complexes displayed sequence selectivity and high-affinity binding to duplex DNA through groove binding [21]. Our research group has reported that the Ru-complexes could stabilize G-rich DNA sequences and induce configurational changes in the DNA, where the planar size of the ancillary ligands of the Ru-complexes has an important function in the stabilization and induction of G-quadruplex structures [22]. In our previous reports, we found that phenanthroline had a better stabilizing effect on G-quadruplex DNA

* Corresponding authors. Tel./fax: +86 20 85220223.
E-mail address: tliuliu@jnu.edu.cn (J. Liu).
[1] These authors contributed equally to this work.

0162-0134/$ – see front matter.
http://dx.doi.org/10.1016/j.jinorgbio.2013.12.005

compared with bipyridyl as an ancillary ligand of the Ru-complex [23–26]. This finding might suggest that the rigid plane of the ligand dominates the interaction of the Ru-complex with the G-quadruplex DNA. Therefore, in the present study, we synthesized and characterized two Ru-complexes: $[Ru(ip)_3](ClO_4)_2\cdot 2H_2O$ (complex 1, ip = 1H-iminazole [4,5-f][1,10] phenanthroline) and $[Ru(pip)_3](ClO_4)_2\cdot 2H_2O$ (complex 2, pip = 2-phenylimidazo-[4,5-f][1,10]phenanthroline), using ip and pip as ancillary ligands, which had larger planarity than those that were previously used for synthesis. The ability of the two Ru-complexes to interact with bcl-2 DNA was investigated. In consideration of the abundance of G-quadruplex DNA, including bcl-2 DNA, telomere DNA, and VEGF, in many kinds of cancer cells, we studied the selectivity of the two complexes for bcl-2 DNA. We found that complex 1 had a stronger selectivity for bcl-2 DNA and a better ability in stabilizing bcl-2 DNA compared with complex 2. Moreover, complex 1 could induce configurational changes in bcl-2 DNA. The results demonstrate that the planar size of an ancillary ligand is a key factor in the interaction of the Ru-complexes with G-quadruplex structures, and an overlarge ligand of this kind of the Ru-complexes might reduce its binding affinity for G-quadruplexes.

To further understand the mechanisms associated with the cellular activities of the Ru-complexes, which had been shown to include potential antitumor activities [27], aspects relating to cytotoxicity, cellular localization of the Ru-complex, apoptosis, caspase activity, and change in mitochondrial membrane potential induced by complex 1 in HeLa cells were analyzed. The results show that complex 1 displays a broad-spectrum anti-proliferative activity for various cancer cells, especially for HeLa cells, and could enter the nucleus effectively. Complex 1 has a function in inducing the depletion of mitochondrial membrane potential and in the activation of caspases, two events which result in cell apoptosis. Herein, the synthesis and the G-quadruplex interaction properties of the two complexes are elucidated.

2. Experimental section

2.1. Reagents and materials

DNA oligomers bcl-2 (Pu23): 5′-GGGCGC GGGAGG AATTGG GCGGG-3′, Mutbcl-2 (MutPu23): 5′-AAACGC AAAAGG AATTAA ACGGG-3′, F27T: 5′-FAM-CGGGCG CGGGAG GAAGGG GGCGGGAGC-TAMRA-3′ (Donor fluorophore FAM is 6-carboxy-fluorescein; Acceptor fluorophore TAMRA is 6-carboxytetramethylrhodamine), VEGF (5′-GGGCGG GCCGGG GGCGGG-3′), HTG21 (5′-TTAGGG TTAGGG TTAGGG TTAGGG-3′) and bcl-2 rev DNA were purchased from Shanghai Sangon. Calf-thymus (CT)-DNA (Sigma; highly polymerized stored at 4 °C; long-term storage at −20 °C). Concentrations of these oligomers were determined by measuring the absorbance at 260 nm wavelength after melting. Single-strand extinction coefficients were calculated from mononucleotide data using a nearest-neighbor approximation [28,29]. The formations of intramolecular G-quadruplexes were carried out as follows: the oligonucleotide samples were annealed in different buffers at 95 °C for 5 min, slowly cooled to room temperature, and then incubated at 4 °C overnight. Buffer A: 10 mM Tris–HCl, pH = 7.4. Buffer B: 10 mM Tris–HCl, 100 mM KCl, pH = 7.4. Buffer C: 10 mM Tris–HCl, 60 mM KCl, pH = 7.4. Other reagents and solvents were purchased commercial sources unless otherwise specified. Doubly distilled water was used to prepare the buffer solutions.

2.2. Physical measurements

^{1}H NMR spectra were recorded on a Varian Mercury-plus 300 NMR spectrometer with [D_6] DMSO as solvent and SiMe4 as an internal standard at 300 MHz at room temperature. Electrospray ionization mass spectrometry (ES-MS) was recorded on a LQC system (Finngan MAT, USA) by using CH3CN as a mobile phase. Microanalysis (C, H, and N) was carried out with an Elementar Vario EL elemental analyzer. UV–visible spectra were obtained by using a Shimadzu MPS-2000 spectrophotometer. Emission spectra were detected by a Shimadzu RF-5000 luminescence spectrometer (Shimadzu, Japan) and CD (circular dichroism) spectra were recorded on a Jasco J-810 spectropolarimeter. FRET (fluorescence resonance energy-transfer) assay was carried out on Light Cycler 2 real-time PCR (polymerase chain reaction) amplifier (Roche). Fluorescent quantitation polymerase chain reaction was tested by Bio-Rad Chrome 4 PCR instrument. Flow cytometry (BD Bioscience, America) was applied in the determination of cell apoptosis and the change of mitochondrial membrane potential and pH was measured by Orion Model 720 A pH.

2.3. Synthesis of ligands and the two complexes

$RuCl_3\cdot nH2O$ (AR) was obtained from the Kunming Institute of Precious Metals. 1,10-phenanthroline, 2,2′-bipyridine, formaldehyde and benzaldehyde were obtained from Sigma. Synthesis of 1,10-phenanthroline-5,6-dione, $[Ru(ip)_3](ClO_4)_2\cdot 2H_2O$ and $[Ru(pip)_3](ClO_4)_2\cdot 2H_2O$ was prepared and characterized according to the literature references [30,31].

2.3.1. Synthesis of the ligand "ip"

A mixture of 1, 10-phenanthroline-5,6-dione (0.525 g, 2.5 mmol), methanal (0.26 ml 36%–38%, 3.5 mmol), ammonium acetate (3.88 g, 50 mmol) and glacial acetic acid (10 mL) was refluxed for 4 h. The cooled deep red solution was diluted with 40 mL water and neutralized with ammonium hydroxide to give a yellow precipitate. The precipitate was collected and purified by column chromatography on silica gel (60–100 mesh) with ethanol as eluent to give the compound as yellow powder. Yield: 0.378 g, 45%. ESI-MS (CH3OH): m/z = 327 ($[M + H]^+$).

2.3.2. Synthesis of the ligand "pip"

The ligand was prepared by a method similar to that of the ligand ip by replacing methanal with benzaldehyde (371 mg, 3.5 mmol). Yield: 88%. ESI-MS (CH3OH): m/z = 297 ($[M + H]^+$).

2.3.3. Synthesis of $[Ru(ip)_3](ClO_4)_2\cdot 2H_2O$

A mixture of $[Ru(bpy)_2Cl_2]\cdot 2H_2O$ (0.26 g, 0.5 mmol), ethylene glycol (10 mL) and ligand ip (0.168 g, 0.5 mmol) was refluxed for 4 h under argon. Upon cooling, a red precipitate was obtained by a dropwise addition of saturated aqueous $NaClO_4$ solution. The precipitated complex dried under vacuum, and purified by chromatography over alumina (200 meshes), using MeCN-acetonitrile (8:1, v/v) as an eluent, yield: 62%. The sample shows good solubility in solvents such as MeCN, DMSO and acetone. ESI-MS (CH3OH): m/z = 761 ($[M\text{-}2ClO_4\text{-}H]^+$), m/z = 381 ($[M\text{-}2ClO_4/2]^{2+}$) ^{1}H NMR. [$(CD_3)_2SO$]: ppm δ9.09 (d, 6H, J = 8Hz), 8.60 (s, 3H, J = 5Hz), 7.97 (d, 6H, J = 5Hz), 7.72 (dd, 6H, J1 = 5Hz, J2 = 3Hz). Anal. Calc.for $C_{43}H_{37}N_{12}Ru$: C, 62.76; H, 4.53; N, 20.43. Found: C, 62.67; H, 4.45; N, 20.01.

2.3.4. Synthesis of $[Ru(pip)_3](ClO_4)_2\cdot 2H_2O$

This complex was synthesized in a manner identical to that described for $[Ru(ip)_3](ClO_4)_2\cdot 2H_2O$, with pip (0.62 g, 2.1 mmol) in place of ip, yield: 68%. ESI-MS (CH3OH): m/z = 989 ($[M\text{-}2ClO_4\text{-}H]^+$), m/z = 495 ($[M\text{-}2ClO_4/2]^{2+}$) ^{1}H NMR [$(CD_3)_2SO$]: ppm δ9.01 (d, 6H, J = 8Hz), 8.43 (d, 6H, J = 8Hz), 8.03 (d, 6H,J = 5Hz), 7.76 (dd, 6H, J1 = 5Hz,J2 = 3Hz), 7.60 (t, 6H, J = 7.5Hz), 7.53 (t, 3H, J = 7.5Hz). Anal. Calc.for $C_{63}H_{54}N_{12}Ru$: C, 70.05; H, 4.98; N, 15.56. Found: C, 70.15; H, 5.12; N, 15.71.

2.4. Fluorescent experiments

For the selectivity assay, 4 μM DNA (CT-DNA, G4-TTA, VEGF or bcl-2 DNA) and 2 μM Ru-complex were adequately mixed in buffer B (10 mM Tris–HCl, 100 mM KCl, pH 7.4) over night in 4 °C. Before the test, the solution was incubated for about 20 min to achieve initial test

temperature. For the titration test, the emission spectra as well as titration curves were recorded through a constant concentration of the Ru-complexes, to which the DNA stock solutions were added step by step at room temperature. The Ru-complex (3000 μL) in a 1.0 cm path length quartz cuvette was loaded into the fluorimeter sample block and the solution was incubated for 5 min before the absorption spectra were recorded. The titration processes were repeated several times until no further change was observed in the spectra. The fluorescent spectra were recorded in wavelength 500 ~ 800 nm by using a Shimadzu RF-5000 luminescence spectrometer (Shimadzu, Japan) at room temperature with excitation wavelength 460 nm. The changes in the Ru-complex concentration caused by dilution at the end of each titration were negligible.

2.5. Continuous variation assessment

The preparation of two series of the solutions for these experiments: one with varying concentrations of the Ru-complex diluted in buffer B, and another one with increasing mole fractions of [Ru-complexes]/[DNA]. The concentration of the Ru–DNA solutions was constant at 10 μM. The emission spectrum was collected from 500 to 750 nm using a quartz cell with a 1 cm path length at 25 °C. The ΔI values were calculated by subtracting the fluorescence intensity of the Ru-complex solution without Pu23 DNA from the fluorescence intensity of corresponding complex solution with Pu23 DNA at λ_{max}. This value was plotted versus the complex mole fraction to obtain a Job plot of ΔI–X. Analysis of the data was carried out using Origin 7.5 (Origin Lab Corp).

2.6. Absorption spectra study

The absorption titrations of the Ru-complexes in buffer B were detected by using a constant Ru-complex concentration (20 μM) to which increments of the DNA stock solution was added. The volume of the Ru-complex was 3000 μL. During the titration, aliquots of a stock solution of Pu23 were also added to each cuvette to eliminate the absorbance value of DNA itself. The solutions were mixed by repeated inversion and incubated for 5 min before detection. The titration processes were repeated several times until no change was observed in the spectra indicating an achievement of binding saturation. Emission spectra of the Ru-complexes in the presence of increasing amounts of bcl-2 DNA in buffer B were recorded in wavelength 230 ~ 650 nm by using a Shimadzu MPS-2000 spectrophotometer at room temperature with excitation wavelength 460 nm. The changes of the Ru-complexes concentration due to dilution at the end of each titration were negligible.

2.7. Chromogenic reaction

This assay was for the preparation of the Ru-complex-promoted G-quadruplex-hemin DNAzyme. In detail, an equal volume of the Ru-complex solution (in water) was added to the DNA solutions (20 μM DNA, 10 mM Tris–HCl, 100 μM EDTA, pH 8.00) allowing the DNA strands to form the G-quadruplex structure within 40 min. Subsequently, an equal volume of hemin (dissolved in DMSO) was dissolved in the above G-quadruplex solutions and kept for 2 h at room temperature to form the DNAzymes. Finally, 180 μL of 296 μM TMB-1.76 mM H_2O_2 was added as the substrate of 20 μL peroxidatic DNAzyme system. The mixture was kept for 1.5 h at room temperature and photographed with a digital camera.

2.8. FRET assay

The fluorescent labeled oligonucleotide F21T was prepared as a 100 μM solution in buffer B and then annealed by heating to 90 °C for 5 min, followed by cooling to room temperature overnight. Fluorescence melting curves were determined with a Bio-Rad iQ5 real-time PCR detection system in a total reaction volume of 20 μL containing 0.2 μM of labeled oligonucleotide and different concentrations of the Ru-complexes. Measurements were made in triplicate on a DNA Opticon Engine (MJ Research) with excitation wavelength at 470 nm and detection at 530 nm. Fluorescence readings were taken at intervals of 1 °C over the range 37–99 °C with a constant temperature being maintained for 30 s prior to each reading to ensure a stable value. For the competitive FRET assay, the F27T (0.4 μM) was mixed with 1 μM of the Ru-complexes and 0, 1 and 20 μM of CT-DNA in buffer B and the measurements were carried out as previously mentioned. Final analysis of the data was carried out using Origin 7.5 (Origin Lab Corp.).

2.9. PCR stop assay

The oligonucleotide bcl-2 (Pu23): 5′-GGGCGCGGGAGGAATTGGGCGGG-3′ and the corresponding complementary sequence (bcl-2rev) were used here. The reactions were performed in 1× PCR buffer, containing 10 pmol of each oligonucleotide, 0.16 mM dNTP, 2.5 U Taq polymerase, and various concentrations of the Ru-complexes. Reaction mixtures were incubated in a thermocycler with the following cycling conditions: 94 °C for 3 min, followed by 30 cycles of 94 °C for 30 s, 58 °C for 30 s, and 72 °C for 30 s. PCR products were then analyzed on 15% native polyacrylamide gels in 1× TBE buffer and silver stained.

2.10. CD study

The CD titration procedure is described as follows: CD titration was performed at a fixed DNA concentration (2 μM) with various concentrations of the Ru-complexes in different buffers. After each addition of the Ru-complexes, the reaction was mixed adequately and allowed to equilibrate for at least 5 min prior to a scan. The spectra were accumulated over the wavelength range of 220 to 330 nm at 25 °C with a bandwidth of 5 nm by using a Jasco J-810 spectropolarimeter. For each sample, the spectrum was scanned at least three times. The instrument was flushed continuously with pure evaporated nitrogen throughout the experiment. The scan for buffer alone was subtracted from the average scan for each sample.

2.11. Cell culture

Cells were cultured in DMEM (Dulbecco's modified Eagle's medium) supplemented with 10% heat inactivated fetal bovine serum, 100 μg mL^{-1} penicillin and 100 μg mL^{-1} streptomycin. Cells were maintained at 37 °C in a 5% CO_2 incubator, and the media were changed every three days.

2.11.1. MTT (3-(4,5-dimethylthiazol-2-yl)-2,5-diphenyltetrazolium bromide) assay

Cell cytotoxicity was determined by measuring the ability of cells to transform MTT to a purple formazan dye after incubation with different Ru-complexes for 48 h. Cells including HeLa, A549, CNE, HepG2 and MDA-MB-231 were incubated to exponential phase, seeded in 96-well culture clusters (Costar) at a volume of 100 μL per well and incubated for 24 h at 37 °C in 5% CO_2. (Cells at exponential growth phase were pre-diluted to 4×10^4 cells mL^{-1}). Then the cells were further incubated with various concentrations of the Ru-complexes (2.5, 5, 10, 20, and 40 μM) for 48 h. After the treatment, MTT (20 μL, 5 mg mL^{-1}) the solution was added to each well. After a further period of incubation (4 h at 37.8 °C in 5% CO_2) the suspension was replaced with DMSO (150 μL/well) to dissolve the formazan. Finally, the plates were analyzed on a microplate reader (SpectroAmaxTM250) at a wavelength of 570 nm (the absorbance of the complexes at this wavelength can be neglected). All data were from at least three independent experiments and expressed as mean ± standard deviation.

2.11.2. Laser confocal microscopy image analysis

HeLa cells were grown on a laser confocal microscopy 35 mm^2 culture dishes at a density of 1.0×10^4 cells under a 5% CO_2 atmosphere for 24 h in 37 °C, then were added in the cell layer. Cells were treated with complex 1 (20 and 6 μM) and incubated for different time intervals (3 h, 6 h and 24 h). Before the imaging, the cell nuclei were stained with Hoechst 33342 (5 μg mL^{-1}) for 20 min. After being washed with PBS (phosphate buffered saline) twice, the cells were cultured in fresh medium on a thermo-cell culture FCS2 chamber of Carl Zeiss Cell Observer (Jena, Germany). Cell images were captured with a monochromatic CoolSNAP FX camera (Roper Scientific, USA) and analyzed by using AxioVision 4.2 software (Carl Zeiss). The Ru-complexes had: 488 nm excitation, detection at 560–615 nm (green) and 625–754 nm (red).

2.11.3. Flow cytometric analysis

HeLa cells in exponential growth were incubated without or with complex 1 at different concentrations (5, 10 and 20 μM) for 24 h, then harvested by trypsinization, washed twice with ice-cold PBS, resuspended in 70% ethanol in PBS, and kept at 4 °C overnight. Before the analysis, the cells were adjusted to a final density of 1×10^6 cells/mL in PBS buffer containing RNase A (1 mg mL^{-1}) and stained with 10 mg mL^{-1} of propidium iodide (PI) in darkness for 30 min at 37 °C. The resulting suspension was then passed through a nylon mesh filter (400 meshes) and analyzed on a Becton Dickinson FACS can. Cell cycle distribution was calculated using the Modifit-3 program.

2.11.4. Assessment of mitochondrial membrane potential

Detection of mitochondrial depolarization was performed by flow cytometry using Mitoprobe JC-1 assay kit (Molecular Probes) according to the manufacturer's instruction. The cells were treated with different concentrations of complex 1 for 24 h after adherence. After the incubation, the cells were washed with warm PBS and resuspended in 0.5 mL of PBS (about 1×10^6 cells mL^{-1}). 10 μg mL^{-1} of JC-1 was added to the cells for 15 min incubation at 37 °C in the dark before analysis. The percentage of the green fluorescence from JC-1 monomers was used to demonstrate the cells that lost mitochondrial membrane potential. The red and green fluorescence intensities of JC-1 dye were measured by flow cytometry. A total of 10,000 events were analyzed for each sample.

2.11.5. Caspase activity assay

Harvested cell pellets were suspended in cell lysis buffer and incubated on ice for 1 h. After a centrifugation at 10,000 *g* for 30 min, the supernatants were collected and immediately measured for protein concentration by a BCA kit. As for caspase activity assay, the cell lysates were placed in 96-well plates and then the specific caspase substrates were added. Ac-DEVD-AMC (N-acetyl-Asp-Glu-Val-Asp-7-amino-4-methylcoumarin) is for caspase-3, Ac-IETD-AMC (Ac-Ile-Glu-Thr-Asp-AMC) is for caspase-8, and Ac-LEHD-AMC (Ac-Leu-Glu-His-Asp-AMC) is for caspase-9. The plates were then incubated at 37 °C for 1 h, and caspase activity was determined by fluorescence intensity with the excitation and emission wavelengths set at 380 nm and 440 nm, respectively.

3. Results and discussion

3.1. Fluorescence selectivity of the Ru-complex between quadruplex DNA and non-quadruplex DNA

The synthesis routes of the two complexes are detailed in the Experimental section, and the mass spectra and ^1H NMR spectra data shown in Fig. S1 and Fig. S2 distinctly confirm the generation of complexes 1 and 2. The structures of complexes 1 and 2 are presented in Fig. 1.

To understand the interaction between the Ru-complex and quadruplex DNA, we firstly investigated the selectivity of the Ru-complex for quadruplex DNA and non-quadruplex DNA. Four different DNA sequences including CT-DNA, HTG21, VEGF and bcl-2 DNA (Pu23) were chosen to react with complexes 1 and 2 to investigate the variations of fluorescence behavior of the two complexes. The selectivities of the two Ru-complexes for different DNA structures were presented by the fluorescence strength which stood for the binding affinities via an emission spectroscopy. As shown in Fig. 2, solutions containing different DNAs performed various emission spectra strength. For complex 1 (Fig. 2A), a slight increase in emission was observed in the presence of CT-DNA, on the contrary, a great increase in emission was displayed in the presence of all G-quadruplex DNA sequences, namely, HTG21, VEGF and bcl-2 DNA. Moreover, the fluorescence intensity of the group treated with bcl-2 DNA was much stronger than that of the other two G-quadruplex DNA sequences. As for complex 2 (Fig. 2B), all groups showed a slight increase in fluorescence regardless of the highest emission strength of the group dealt with bcl-2 DNA. These results were attributed to the different affinity abilities of DNA for the Ru-complexes and indicated that there was a greater overlap between the aromatic surfaces of the metal complexes and the bases allowing their interaction when bound to quadruplex as opposed to the duplex DNA [20,32]. Both complexes 1 and 2 harbored the best selectivity for G-quadruplex sequences especially for bcl-2 DNA while complex 1 performed better than complex 2. As we know the ligand of complex 2 has a better stretched planarity than that of complex 1, however, the

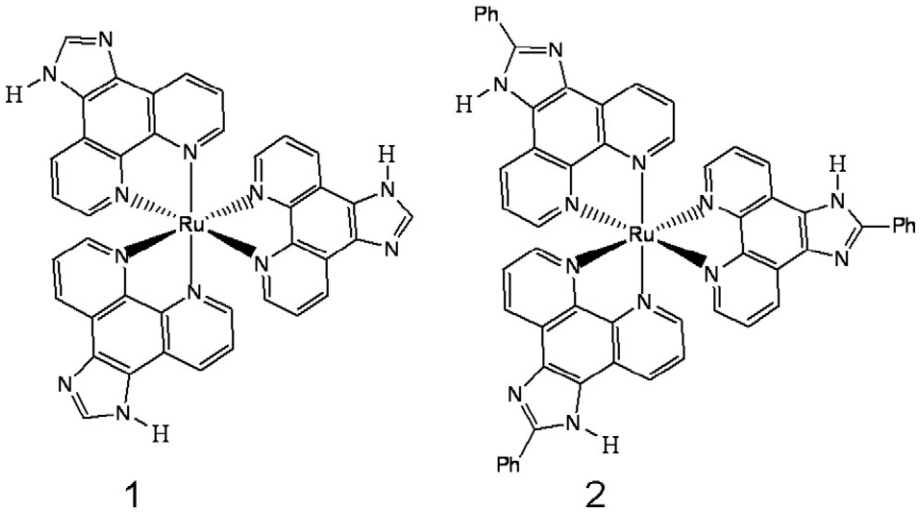

Fig. 1. Structures of the two Ru-complexes: $[Ru(ip)_3](ClO_4)_2 \cdot 2H_2O$ (1), $[Ru(pip)_3](ClO_4)_2 \cdot 2H_2O$ (2).

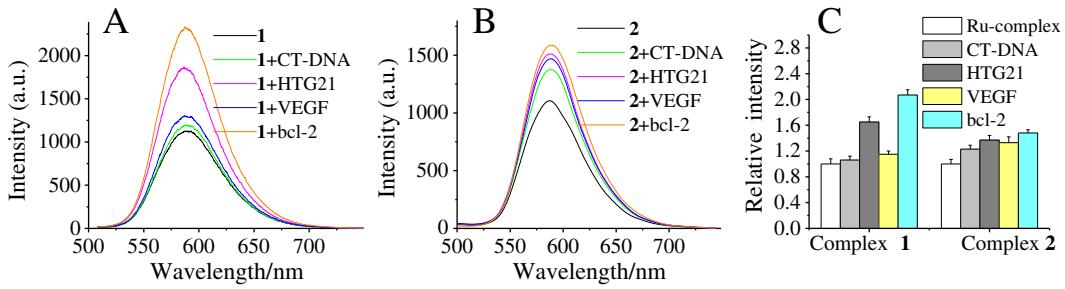

Fig. 2. Selectivity of the Ru-complex between quadruplex DNA and non-quadruplex DNA. Complexes 1 (A) and 2 (B) were mixed with CT-DNA, HTG21, VEGF and bcl-2 DNA (Pu23) in Tris-KCl buffer (10 mM Tris–HCl, 100 mM KCl, pH 7.4) respectively. [Ru-complex] = 2 μM, [DNA] = 4 μM. (C) The relative fluorescence strength of complexes 1 and 2 without or with different DNA sequences depicted in a histogram.

observation indicated that the ligand of complex 1 had a better affinity ability for bcl-2 DNA than that of complex 2. Considering our previous study that a greater planar area of the ancillary ligand always showed a higher binding affinity for quadruplex DNA [24], we infer that only a moderate planarity ligand of the Ru-complex will exhibit the best affinity ability to bcl-2 DNA. Definitely, it needs to be further verified by more studies.

3.2. Binding ability of the Ru-complex with quadruplex DNA

In terms of the above results, we chose Pu23 as the object for a further understanding of the interaction mechanism. The emission spectra of complexes 1 (Fig. 3A) and 2 (Fig. 3B) in the presence of increasing amounts of Pu23 in 10 mM Tris–HCl buffer, 100 mM KCl (pH = 7.4) were determined. Fluorescence intensities increased gradually with the incremental concentration of DNA and the extent of fluorescence intensity enhancement (I/I_0) was 2.37 and 1.57 respectively for complexes 1 and 2, which further illustrated that complex 1 showed a stronger interaction with Pu23. In general, complex 1 shows high selectivity and affinity ability to bcl-2 DNA.

To further validate the meaningful binding stoichiometries of the Ru-complexes with quadruplex DNA, we analyzed continuous variation using the luminescence intensities. As shown in Fig. 3C, the X values of the point of intersection for complexes 1 and 2 with bcl-2 G-quadruplex were 0.6 and 0.51, respectively. This result indicated that complex 1 or 2 could bind to bcl-2 DNA (Pu23) by a 3:2 or 1:1 binding stoichiometric ratio.

3.3. Biding absorption spectra studies

Although the fluorescence experiments authenticated the real interaction between the Ru-complex and Pu23, it was still necessary to further investigate the particular mechanism of the interaction.

Absorption spectra measurements were always used to further clarify the nature of the interaction between these Ru-complexes and G-quadruplex DNA (Pu23). The absorption spectra of these complexes dealt with DNA were shown in Fig. 4. With an increasing addition of DNA, both complexes displayed hypochromism around 460 nm and 280 nm, which were conceived as the metal-to-ligand charge transfer band (MLCT band) and intraligand absorption band (IL band). As hypochromism is usually observed when a complex binds to DNA through intercalation because of the strong stacking interaction between an aromatic chromophore and the DNA base pairs in the intercalation mode, so the extent of hypochromism indicates the intercalation binding strength [33,34]. The absorbance spectra were recorded after each addition. As for complex 1, the values of ΔH (%) were calculated to be 15.9% (around 460 nm) and 22.3% (around 280 nm) respectively. Likewise, the values of ΔH (%) for complex 2 were calculated to be 9.1% (around 460 nm) and 29.6% (around 280 nm) respectively. The MLCT bands and IL band of complexes 1 and 2 showed hypochromism but no obvious bathochromism. However, another narrow separated band at about 263 nm was present in complex 1 (the second arrow in Fig. 4A). This result indicated probably that the two complexes could intercalate the G-quadruplex through a π–π stacking interaction. In order to compare the DNA-binding affinities of the two complexes quantitatively, their intrinsic DNA-binding constants (K_b) were calculated by monitoring the changes of the MLCT absorbance of the two complexes according to the Scatchard equation (Eqs. (1a) to (1c)).

$$C_b = C_t\ddot{A}n(F-F_0)/(F_{max}-F_0) \quad (1a)$$

$$r = C_b/C_{DNA} \quad (1b)$$

$$r/C_f \; nK_b - rK_b \quad (1c)$$

Here, C_t is the total compound concentration, F being the observed fluorescence emission intensity at a given DNA concentration, F_0 being the intensity in the absence of DNA, and F_{max} is the fluorescence of the totally bound compound. Binding data were cast into the form of a

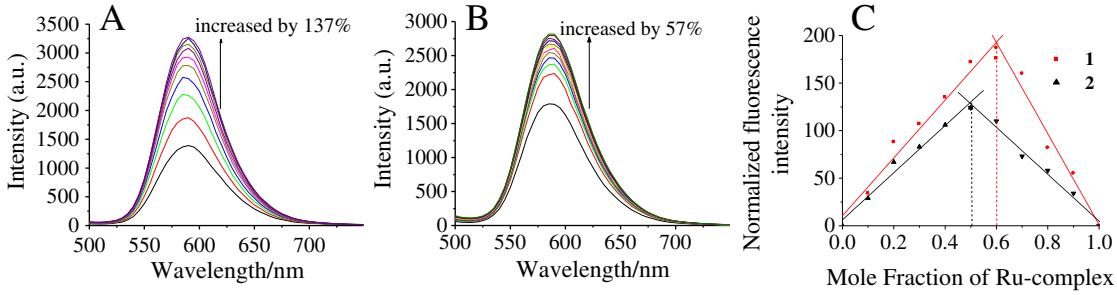

Fig. 3. Emission spectral traces of complexes 1 (A) and 2 (B) in Tris-KCl buffer (10 mM Tris–HCl, 100 mM KCl, pH 7.4) at increasing ratios of [Pu23]/[Ru-complex], [Ru-complex] = 2 μM, [Pu23] = 0–10 μM, EX = 467. Arrows show the emission intensity changes upon increasing DNA concentrations. (C) Job plot using luminescence data for complexes 1 and 2 with bcl-2 DNA in 10 mM Tris–HCl buffer, 100 mM KCl (pH = 7.4). Total concentration was maintained at 1 μM, the stoichiometries of complexes 1 and 2 with bcl-2 DNA were about 3:2, 1:1 respectively.

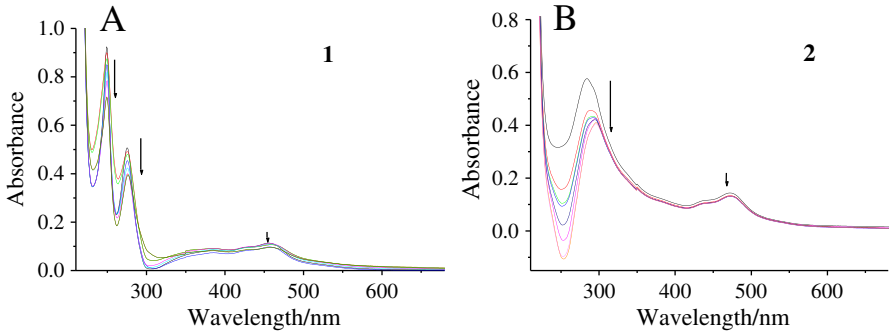

Fig. 4. Absorption spectra of complexes 1 (A) and 2 (B) ([Ru-complex] = 10 μM) in the presence of Pu23 in Tris-KCl buffer (10 mM Tris–HCl buffer, 100 mM KCl, pH = 7.4, [Pu23] = 0–14 μM). Arrows indicate the changes in absorbance with increasing DNA concentrations. These results are mean values of at least three independent experiments.

Scatchard plot of r/C_f versus r, where r is the binding ratio C_b/[DNA], and C_f is the free ligand concentration [28]. The intrinsic binding constants K_b of complexes 1 and 2 were $1.05 \pm 0.4 \times 10^6$ M^{-1} and $4.7 \pm 0.03 \times 10^5$ M^{-1} (Table 1). The binding constant K_{b1} (binding constant of complex 1) was larger than K_{b2} (binding constant of complex 2) indicating that complex 1 bound to the DNA more tightly than complex 2 did. All the absorbance spectra were well consistent with the result of the emission spectroscopic analysis. The higher binding affinity of complex 1 probably results from the fact that its ancillary ligand can intercalate with the base pairs or enter into the grooves within DNA more easily [21,35,36].

3.4. Visual detection of G-quadruplex structures induced by the Ru-complexes

As we have investigated the interaction between the Ru-complexes and bcl-2 DNA (Pu23), it was necessary to further study the new DNA structure evoked by the Ru-complexes.

Although certain kinds of G-rich sequences have been demonstrated to form G-quadruplex structures readily at physiological concentrations of Na^+ and K^+ in vitro [37–40], the existence of G-quadruplex structures in vivo is still controversial [41,42]. The determination of G-quadruplex structures has great significance for cancer research and drug development for the lack of direct evidence of this quadruplex structure in living cells. Then we conducted a facile and visual approach to detect the existence of G-quadruplexes with the naked eyes.

It is well known that most G-quadruplex DNA can be effectively induced by K^+, and G-quadruplexes have the ability to bind with hemin to form peroxidase-like DNAzymes which can catalyze H_2O_2-mediated oxidation of TMB (3,3′,5,5′-tetramethylbenzidine). As shown in Fig. 5, the bcl-2 DNA-treated mixture produced DNAzymes to catalyze H_2O_2-mediated oxidation of TMB to show an easily identified color change in the presence of K^+, complex 1 or 2. However, a similar color change failed to emerge in the CT-DNA mixture in the absence or presence of complexes 1 and 2. In conclusion, both complexes could induce bcl-2 DNA into G-quadruplex structures as well as K^+. But for complexes incubated with double strand DNA (CT-DNA), the final solution retained the original color. Obviously, the CT-DNA sequence cannot form the G-quadruplex structure even in the presence of the Ru-complexes.

Table 1
Absorption spectra and hypochromism of complex 1 and 2.

Complex	λ_{max}(free) [nm]	λ_{max}(bound) [nm]	$\Delta\lambda$ [nm]	ΔH [%]	K_b [10^6 M^{-1}]
	457	459	2	15.9	
1	275	276	1	22.3	1.05 ± 0.4
	249	250	1	22.6	
2	472	473	1	9.1	0.47 ± 0.03
	284	296	12	29.6	

3.5. Analysis of bcl-2 G-quadruplex selectivity and binding stability via FRET assays

The thermodynamic selectivity and stabilization activity of complex 1 to G-quadruplex DNA were studied using FRET melting experiment which has come across as a useful tool to characterize the selectivity of binding ligand toward quadruplex structure over the duplex [43]. We firstly used the FRET measurements to determine the selectivity of complex 1 to G-quadruplex DNA and the competitive binding property of CT-DNA. In a system that contained 0.4 μM F27T oligonucleotide and 1 μM complexes, the melting temperatures increased roughly by 13.1 °C and 6.0 °C respectively (Fig. 6A–C). Interestingly, with an addition of increasing amounts of CT-DNA, no significant change in the melting temperatures was observed even at 20 μM CT-DNA. These results indicated that the Ru-complexes exhibited prompt selectivity to bind to G-quadruplex structures and not to other duplex DNA.

To further quantify the stabilization of the complexes for bcl-2 DNA, we conducted another FRET melting assay. Shown in Fig. 6D–E, the melting temperature (T_m) of the G-quadruplex in the absence and presence of increasing amounts of complexes varied obviously. The T_m of the DNA sequence increased in a dose-dependent manner and reached a summit value when r was 2. The relevance of ΔT_m (the enhanced melting temperature) vs "r" was depicted in Fig. 6F, obviously, ΔT_m (1) was much higher than ΔT_m (2) which was 18.0 °C and 7.9 °C respectively. All these results showed that complex 1 had a better stabilization for the G-quadruplex, which was consistent with the results of absorption titration studies showing that complex 1 had the highest K_b (intrinsic DNA-binding constant) value.

3.6. PCR stop assay

In order to further evaluate the efficiency of the complexes stabilizing G-quadruplex DNA, a PCR stop assay was used to ascertain whether these complexes were bound to a test oligomer bcl-2 DNA and mutbcl-2 DNA. Fig. 7A illustrated that in the presence of complex 1, the template sequence could form G-quadruplex structures unable to amplify to the PCR product. Moreover, the inhibitory effect of complex 1 was enhanced clearly as the concentration increased from 1.0 to 8.0 μM with even no PCR product detected at an 8.0 μM concentration. However, complex 2

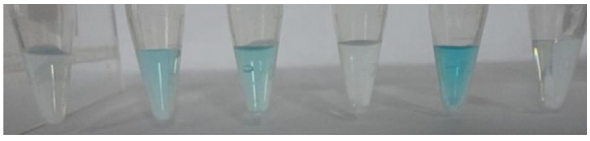

Fig. 5. Characterizations of the DNAzyme functions of bcl-2 DNA (Pu23) and CT-DNA in the presence of K^+ (2 mM) and complexes 1 and 2 (500 nm) in the TMB-H_2O_2 system. Conditions: TMB, 266 mM in Tris-MES buffer (25 mM MES, pH 5.10); H_2O_2, 794 mM; DNA, 500 nM; hemin, 500 nM.

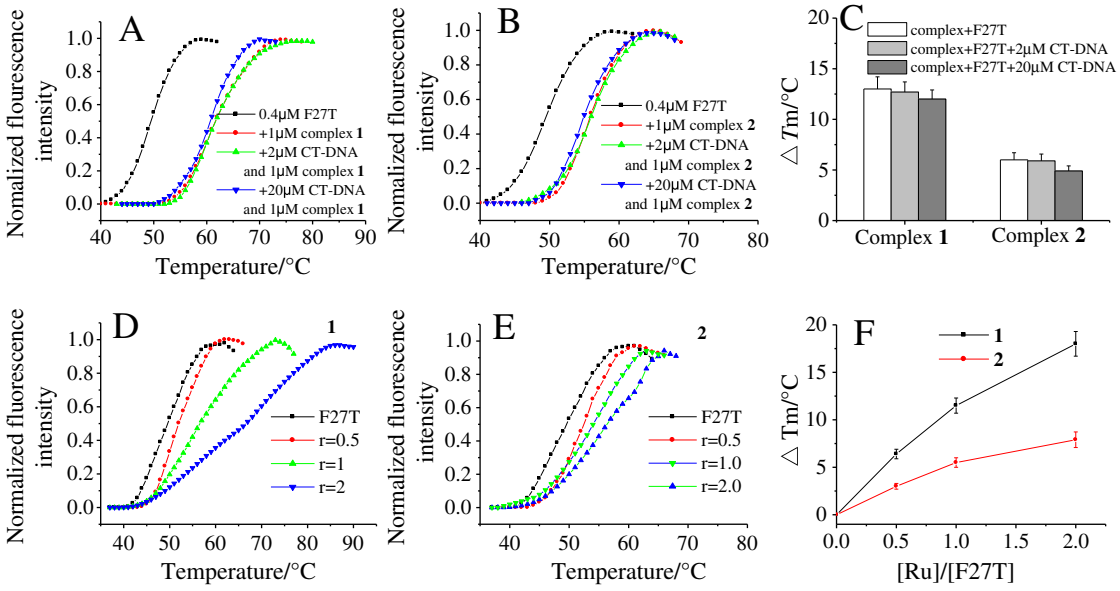

Fig. 6. Bcl-2 G-quadruplex selectivity and binding stability of the Ru-complexes. (A–C) Competitive FRET melting curves of F27T (0.4 μM) with 2 μM of the Ru-complexes and 0, 5 and 50 μM of CT-DNA in 10 mM Tris–HCl buffer containing 60 mM KCl. (D–F) The FRET melting curves for experiments carried out with F27T (1 μM in 10 mM Tris–HCl, 60 mM KCl, pH 7.4) and complexes 1 and 2.

hardly inhibited the appearance of the PCR product with a low concentration. These data suggested that complex 1 was an efficient G-quadruplex binder and inducer even at a low concentration. Besides, in order to exclude the possibility of enzyme inhibition by the complexes, the parallel experiment was performed using a mutated oligomer (mutbcl-2 DNA, Fig. 7B) instead of bcl-2 DNA in identical conditions. And the results indicated that these complexes could not obviously inhibit the Taq polymerase at a comparable concentration. In general, complex 1 can stabilize G-quadruplex structure more efficiently than complex 2 does.

3.7. CD spectra analysis

CD spectroscopy is used to investigate the conformational properties of the enantiomeric chiral molecules in relation to the G-quadruplex DNA. Although CD cannot give precise structures of these G-quadruplexes, it can be used to distinguish parallel and antiparallel G-quadruplex structures depending on their strand orientation [44–46].

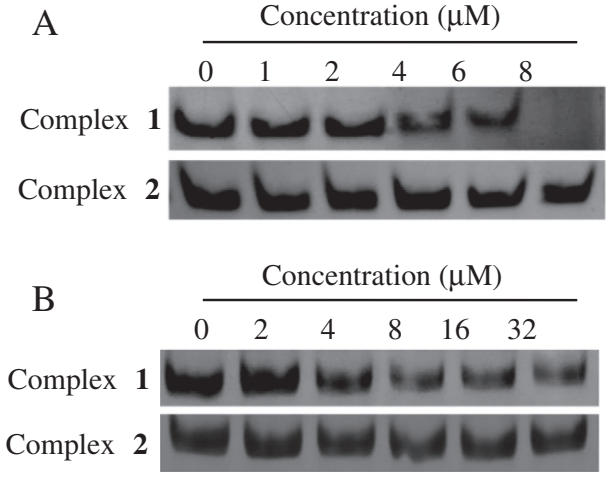

Fig. 7. Effect of the Ru-complexes on the hybridization of bcl-2 DNA (A) and mutbcl-2 DNA (B) in the PCR stop assay. Complexes 1 and 2 were at 0–15 μM concentrations.

In the absence of salt, the CD spectrum of bcl-2 DNA exhibited a negative band at 240 nm as well as a major positive band at 260 nm at room temperature, which probably corresponded to the signal of the bcl-2 DNA random coil. A minor positive band near 295 nm was also observed. Upon titration with complex 1, dramatic changes in the CD spectra were observed. Bands at 240 and 265 nm gradually disappeared with the addition of the complex and eventually led to the appearance of a positive band at 240 nm and a major negative band at 260 nm. Meanwhile, a new, strong, positive band gradually appeared near 285 nm (Fig. 8A). It implied that complex 1 could stabilize the combination of bcl-2 G-quadruplex and tended to form the antiparallel conformation. However, upon addition of complex 2, the bands at 240 and 265 nm only had the dose-dependent changes of strength (Fig. 8B). The results indicated that complex 2 could only stabilize the combination of bcl-2 G-quadruplex to some extent but failed to form the antiparallel G-quadruplex conformation. In the presence of K^+, bcl-2 DNA can form the hybrid-type G-quadruplex structure [47]. The CD spectrum of such preformed structure showed a strong positive band at 290 nm, 265 nm, and a negative band at 235 nm (Fig. 8C, black line). Upon titration of complex 1 into this DNA solution, the CD spectra changed with a weak enhancement of the band at 235 nm and a slight decrease of the band at 265 nm and at 290 nm (Fig. 8c). By contrast, the addition of increasing amounts of complex 2 to bcl-2 DNA in 100 mM KCl buffers resulted in no significant changes in the CD spectra (Fig. 8D). The results indicated that complex 1 was more efficient in inducing the formation of G-quadruplexes compared with complex 2.

These data implied that the conformation of the G-quadruplex was stabilized by K^+, and neither of the two Ru-complexes could change the conformation of the G-quadruplex in the presence of high ionic strength.

In the Tris–HCl buffer solution, the CD spectrum of this structure in the absence of any complex showed a strong positive band at 261 nm, and a major negative band at 249 nm. The signals demonstrated that the conformations of mutbcl-2 were in disorder, not in an orderly secondary structure. Upon titration of complex 1 or complex 2, the CD spectra produced scarce changes (Fig. 8E,F). No significant change in

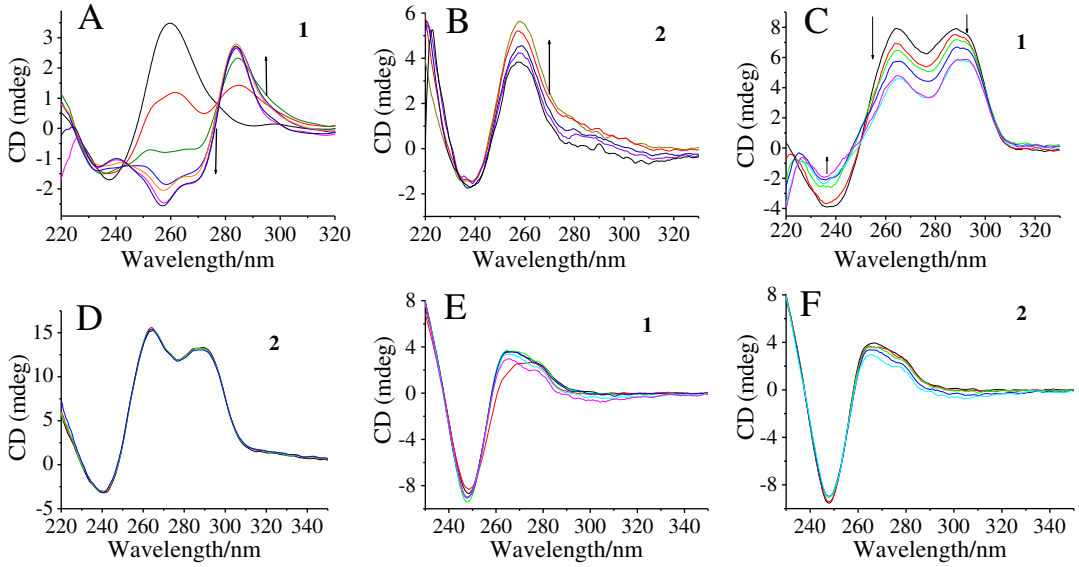

Fig. 8. CD spectra of bcl-2 DNA (Pu23) in 10 mM Tris–HCl buffer (pH = 7.4) (A, B) and in 100 mM KCl buffer (pH = 7.4) (C, D) in the presence of increasing amounts of complexes 1 and 2. (E, F) CD spectra of mut bcl-2 DNA in 10 mM Tris–HCl buffer (pH = 7.4) in the presence of increasing amounts of complexes 1 and 2. [Ru-complex] = 0–12 μM, [DNA] = 2 μM.

the CD spectrum was observed even in elevated concentrations of the complex. The results illustrated that the two complexes could not induce mutbcl-2 DNA to form a G-quadruplex structure and scarcely interacted with mutbcl-2 DNA.

3.8. In vitro cytotoxicity analysis

In vitro assay, we firstly investigated the antitumor property of the Ru-complexes using the MTT assay in five types of cancer cells, namely, human cervical cancer (HeLa), human lung carcinoma (A549), nasopharyngeal carcinoma cell (CNE), human hepatocellular liver carcinoma (HepG2), and human breast cancer (MDA-MB-231) cells.

As shown from Table 2, the IC_{50} values varied obviously between different complexes for a certain cell line. It could be concluded that complex 1 had the most efficient anticancer performance compared with complex 2 in most human cancer cell lines. Most of the tested cancer cell lines were susceptible to complex 1 particularly the HeLa cells which were half inhibited at 11.2 μM treatment concentration. The morphology changes of HeLa cell induced by complex 1 were also presented by the light microscope (Fig. 9). With increasing concentrations of complex 1, lots of cells became round, detached cells increased and adherent cells gradually decreased, then a large number of suspended cells appeared, even accompanied with cell debris. In particular, both complexes showed weak cytotoxicity against the normal cells (NIH/3T3) with IC_{50} values at 183.3 μM and 92.0 μM (not listed in the Table 2).

In brief, all these results indicated that the complex had relatively higher selectivity to cancer cells than to normal cell lines and complex 1 exerted well anti-proliferative activity especially in HeLa cells, which led this Ru-complex to a good application potential in cancer chemoprevention and chemotherapy.

Table 2
IC_{50} of complexes 1 and 2 in various human cancer cells.

Complex	IC_{50} (μM)				
	HeLa	A549	CNE	HepG2	MDA-MB-231
1	11.2 ± 0.5	26.4 ± 1.2	39.3 ± 0.4	11.6 ± 0.3	24.4 ± 1.1
2	22.6 ± 1.0	74.6 ± 2.8	121.0 ± 4.5	32.8 ± 0.6	14.6 ± 0.7

3.9. Cellular uptake by laser confocal microscopy

The Ru-complex is an autofluorescent complex that emits green fluorescence and red fluorescence and allows for the visualization of its intracellular presence in living cells by laser confocal microscopy [48]. To investigate the intracellular accumulation of complex 1, we examined its fluorescence in HeLa cells after incubation for 3, 6 and 24 h. The intracellular green fluorescence was remarkably high in cells after 3 h of treatment, followed by a progressive increase to 6 h. As shown from the upper panel (Fig. 10A), complex 1 mostly entered the cytoplasm within 3 h. However, the Ru-complex concentrated well in the nucleus within 6 h at 20 μM instead of 5 μM (Fig. 10B). This result suggested that complex 1 might enter the nucleus to interact with DNA after a 6 h treatment, but the Ru-complex couldn't enter the nucleus well at a too low concentration. The abilities of the complex to enter the nuclei might be related to its appropriate hydrophobic ligand and its affinity for the constituents of the nucleus. By the way, the cells appeared to be dying after 24 h incubation with complex 1 (20 μM), which indicated that the accumulation of this Ru-complex in the nucleus of HeLa cells might lead to the inhibition of DNA transcription and translation resulting in cell death. Therefore, these results revealed that the nucleus was one of the cellular targets of the Ru-complex and complex 1 displayed promising anticancer activities.

3.10. Apoptosis and cell cycle arrest induced by complex 1

As we know, the inhibition on cancer cell proliferation by anticancer drugs could be the results of induction of apoptosis or cell cycle arrest, or a combination of these two modes. Therefore, we performed PI-flow cytometric analysis to study the potential mechanisms involved in the cell death induced by complex 1. The results revealed that exposure of HeLa cells to different concentrations of complex 1 led to a dose-dependent increase in sub-G1 cell population which was a symbol of apoptosis (Fig. 11). However, the proportion of G0/G1 phases increased in a dose-dependent way, which increased up to 71.15% while that of the control group was only 54.73%. By the way, no significant changes in S and G2/M phases were observed in treated cells even in a high treatment concentration. These results indicated that the mode of cell death induced by complex 1 might be a combination of cell apoptosis and cell cycle arrest.

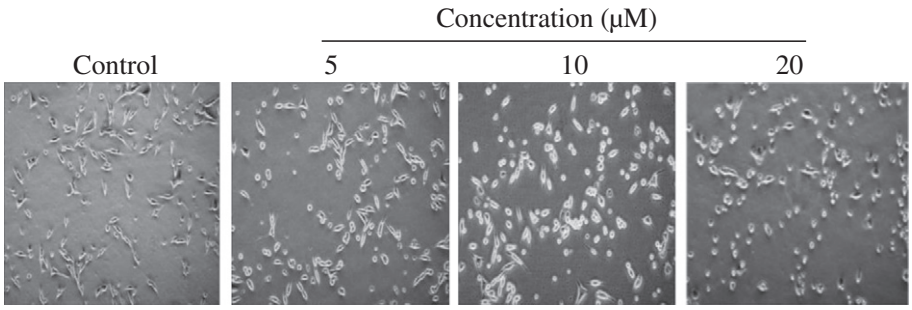

Fig. 9. Effect of the Ru-complexes on cell morphology in HeLa cells. Light microscope examination of HeLa cells was performed after a 48 h treatment with various concentrations of the Ru-complex. Photographs shown are representative of at least three such fields of view per sample, and three independent samples.

3.11. Mitochondria dysfunction and caspase-dependent apoptosis induced by complex 1

Mitochondria play crucial roles in apoptotic signals originating in both the extrinsic and intrinsic apoptotic pathways. Mitochondrial dysfunction is the major key in triggering various apoptotic pathways associated with the initiation of apoptotic cascades [49,50]. Thus, the status of mitochondrial membrane potential was investigated in complex 1-treated HeLa cells to further study the mechanism of apoptosis by JC-1 flow cytometric analysis.

As shown in Fig. 12A, complex 1 induced a dose-dependent increase in the depletion of mitochondrial membrane potential in HeLa cell lines, as evidenced by the shift of fluorescence from red to green. The percentage of depolarized mitochondria in HeLa cells exposed to 10 and 20 μM complex increased from 3.4% (control) to 29.1% and 39.4%, respectively. The induced loss of mitochondrial membrane potential resulted in the release of mitochondrial content and apoptosis-related factors such as cytochrome c and other apoptosis-inducing factors, then DNA damage occurred.

As the loss of mitochondrial membrane potential was associated with the activation of caspase, we determined the activities of initiator caspases (caspase-8 and caspase-9) and effector caspase-3. Fig. 12B showed that complex 1 caused activations of caspase-3, caspase-8, and caspase-9 in the HeLa cells in a dose-dependent manner, which suggested that both intrinsic and extrinsic apoptotic pathways were involved in the apoptosis. The activity of caspases-3, 8 and 9 increased significantly in response to the complex treatments, which indicated that the role of mitochondria in the induction of cell apoptosis was likely to be very important. To further evaluate the roles of caspases in the induced apoptosis, several caspase inhibitors such as z-VAD-fmk (general caspase inhibitor), z-IETD-fmk (caspase-8 inhibitor) and z-LEHD-fmk (caspase-9 inhibitor), were used to examine their effects on the induced cell apoptosis. As shown from Fig. 12C, the induced cell apoptosis was remarkably suppressed by pretreatment with z-VAD-fmk in complex 1-induced cell death, suggesting that complex 1 induced a caspase-dependent apoptosis. Cell apoptosis was also suppressed by caspase-8 inhibitor from 24.43% to 8.5%, which confirmed the contribution of death receptors to the cell apoptosis. Moreover, caspase-9 inhibitor significantly decreased apoptotic cell death to 9.5% indicating the important role of the intrinsic mitochondrial-mediated apoptotic pathway in complex 1-induced apoptosis. In general, all the results confirmed that complex 1 might promote apoptosis through the mitochondria-mediated and caspase-activated pathway in HeLa cells.

4. Conclusions

In this study, we designed and synthesized the two Ru-complexes for consideration as promising candidates for selective targeting of G-quadruplexes. The results revealed that both the Ru-complexes are capable of inducing and stabilizing the bcl-2 G-quadruplex. They also had a very strong binding affinity with significant specificity for quadruplex over duplex interactions. Complex 1 showed a stronger ability in stabilizing and higher efficiency in inducing the formation of G-quadruplexes compared with complex 2, which had an overlarge ligand planar conformation. These distinctions between complex 1 and complex 2 prove that the planar conformation of their cores is crucial for their binding affinities with G-quadruplex for this kind of complex.

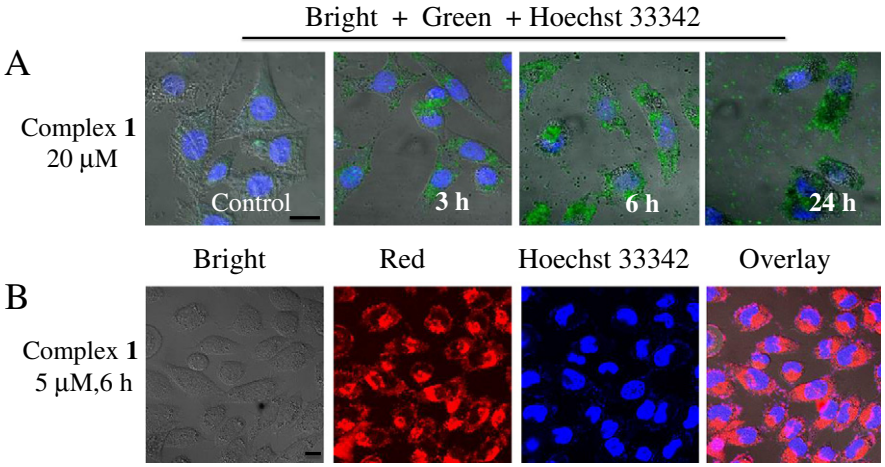

Fig. 10. Cellular localization of the Ru-complex by laser confocal microscope. The upper panel (A) is the real-time imaging of the HeLa cells treated with complex 1 (20 μM). Nuclei and complex 1 were visualized by blue and green fluorescence, respectively; scale bar: 10 μm. The lower panel (B) shows the cellular localization of complex 1 (5 μM) within 6 h in HeLa cells. Nuclei and complex 1 were visualized by blue and red fluorescence, respectively; scale bar: 10 μm.

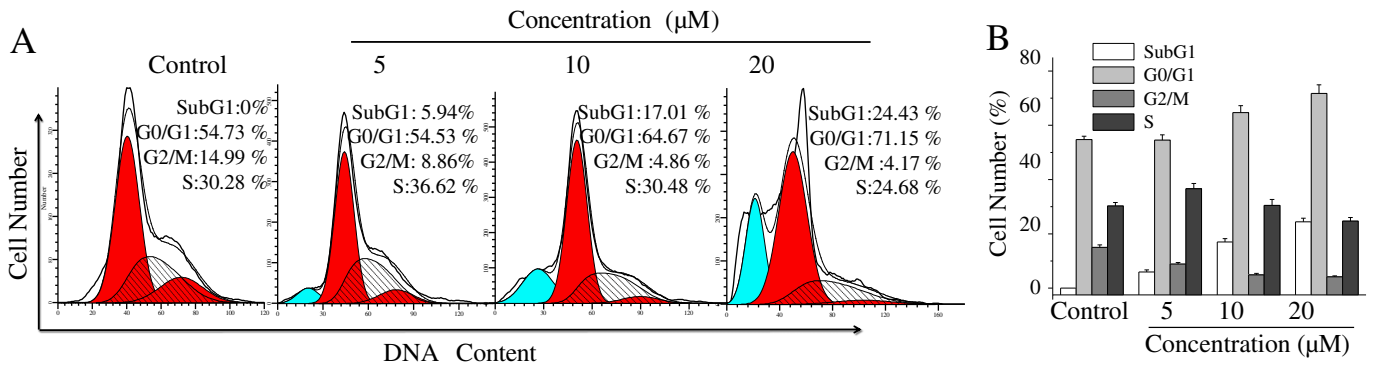

Fig. 11. Effects of complex 1 on cell apoptosis and cell cycle distribution in HeLa cells. (A) The cells treated with different concentrations of complex 1 for 48 h were collected and stained with PI after fixation as described in the Experimental section. (B) Cellular DNA histograms were analyzed by the MultiCycle software. Each value represents the mean of three independent experiments.

Considering our previous studies that showed that a better stretched ligand planarity of the Ru-complexes always facilitated the induction and stabilization of G-quadruplexes [24], we concluded that an undersized or oversized planar conformation for a Ru-complex might not benefit bcl-2G-quadruplex targeting. In effect, a Ru-complex ligand should have the following characteristics: (i) medium size, (ii) high selectivity for quadruplex structures, (iii) high specificity characterized by high binding affinity for G-quadruplexes, (iv) low cytotoxicity, and (v) minimal side effects.

With respect to the high G-quadruplex selectivity of the Ru-complexes, it was inferred that they might be able to affect the biological properties of cells through regulation of gene expression. In the present study, the biological activities of the Ru-complexes in carcinoma cells were tested. Interestingly, complex 1 displayed a broad-spectrum anti-proliferative activity for various cancer cells, especially for HeLa cells, and could partially enter the nucleus in 3 h to 6 h. Then, by flow cytometry, the induction of apoptotic cell death and G0/G1 cell cycle arrest was found as probable causes for the inhibition of HeLa cell growth. Further investigation showed that complex 1 also induced mitochondria-mediated apoptosis by obviously depleting mitochondrial membrane potential, which was further confirmed by the results of caspase activation. The detailed mechanism of cell apoptosis

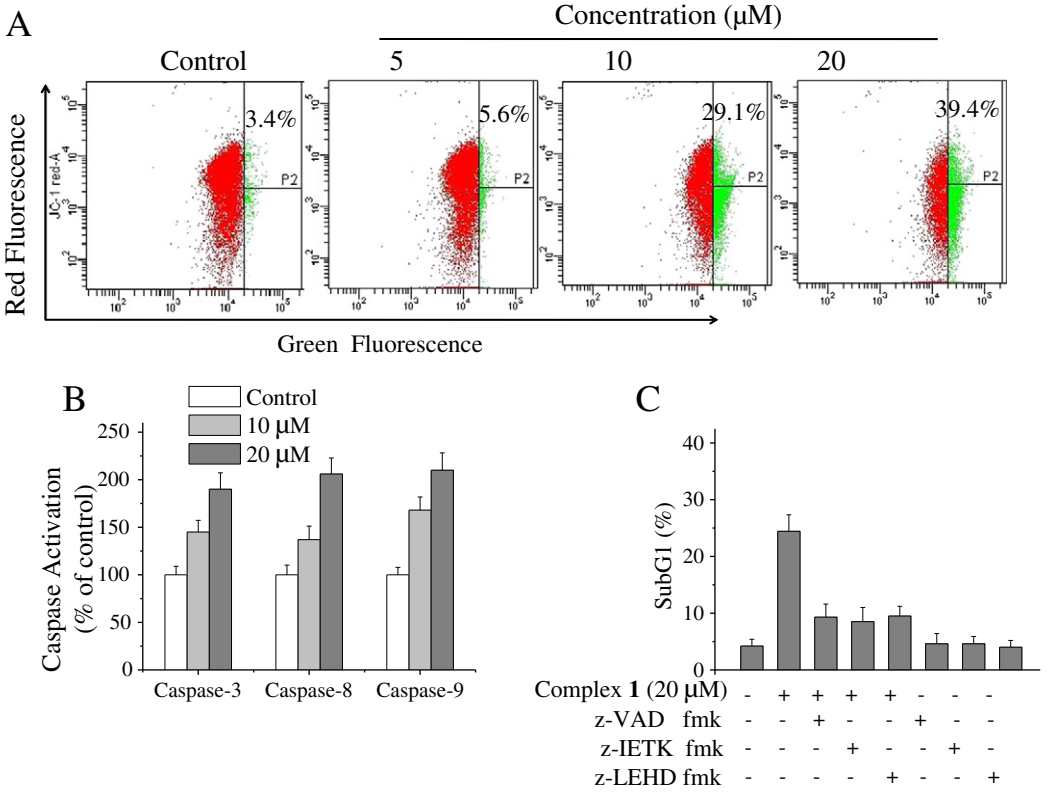

Fig. 12. Complex 1 induces mitochondria-mediated and caspase-dependent apoptosis in HeLa cells. (A) Complex 1 induces depletion of mitochondrial membrane potential. Cells treated with complex 1 for different concentrations were analyzed by JC-1 flow cytometry. (B) Complex 1 induced caspase activation. Cells were treated with complex for 24 h. Significant difference between treatment and control groups is shown. (C) Effects of caspase inhibitors (40 μ M) on apoptosis induced by complex 1. Cells were pretreated with z-VAD-fmk (general caspase inhibitor), z-IETD-fmk (caspase-8 inhibitor), and z-LEHD-fmk (caspase-9 inhibitor) for 2 h followed by co-incubation with complex 1 for 24 h. Apoptotic cells were determined by flow cytometry.

and the relationship between the stabilization of bcl-2 G-quadruplex and cell apoptosis induced by complex 1 are currently under further investigation. Based on all our results, we suggest that this Ru-complex can be a good candidate for selective targeting of bcl-2 G-quadruplex. This complex must be further evaluated for its efficacy as a chemopreventive and chemotherapeutic agent for human cancers.

Abbreviations

G-quadruplex Guanine quadruplex
bcl-2 b-cell lymphoma-2
Ru-complexes Ruthenium(II) complexes
complex 1 $[Ru(ip)_3](ClO_4)_2 \cdot 2H_2O$ (1)
complex 2 $[Ru(pip)_3](ClO_4)_2 \cdot 2H_2O$ (2)
CT-DNA Calf thymus DNA
bpy 2,2′-bipyridine; ip:1H-imidazole[4,5-f][1,10]phenanthroline
pip 2-phenylimidazo-[4,5-f][1,10]phenanthroline
MLCT band Metal-to-ligand charge transfer band
IL band Intraligand absorption band
TMB 3,3′,5,5′-tetramethylbenzidine
FRET Fluorescence Resonance Energy-Transfer
PCR Polymerase chain reaction
CD Circular dichroism
MTT 3-(4,5-dimethylthiazol-2-yl)-2,5-diphenyltetrazolium bromide
PBS Phosphate buffered saline
Ac-DEVD-AMC N-Acetyl-Asp-Glu-Val-Asp-7-amino-4-methylcoumarin
Ac-IETD-AMC N-Acetyl-Ile-Glu-Thr-Asp-7-amino-4-methylcoumarin
Ac-LEHD-AMC N-Acetyl-Leu-Glu-His-Asp-7-amino-4-methylcoumarin

Acknowledgments

This work was supported by the National Natural Science Foundation of China (20871056, 21171070, and 21371075), the Planned Item of Science and Technology of Guangdong Province (c1011220800060, c1211220800571), the Natural Science Foundation of Guangdong Province and the Fundamental Research Funds for the Central Universities.

Appendix A. Supplementary data

Supplementary data to this article can be found online at http://dx.doi.org/10.1016/j.jinorgbio.2013.12.005.

References

[1] J. Dai, T.S. Dexheimer, D. Chen, M. Carver, A. Ambrus, R.A. Jones, D. Yang, J. Am. Chem. Soc. 128 (2006) 1096–1098.
[2] A.T. Phan, Y.S. Modi, D.J. Patel, J. Am. Chem. Soc. 126 (2004) 8710–8716.
[3] D. Sun, K. Guo, J.J. Rusche, L.H. Hurley, Nucleic Acids Res. 33 (2005) 6070–6080.
[4] R. De Armond, S. Wood, D. Sun, L.H. Hurley, S.W. Ebbinghaus, Biochemistry 44 (2005) 16341–16350.
[5] S. Rankin, A.P. Reszka, J. Huppert, M. Zloh, G.N. Parkinson, A.K. Todd, S. Ladame, S. Balasubramanian, S. Neidle, J. Am. Chem. Soc. 127 (2005) 10584–10589.
[6] H. Fernando, A.P. Reszka, J. Huppert, S. Ladame, S. Rankin, A.R. Venkitaraman, S. Neidle, S. Balasubramanian, Biochemistry 45 (2006) 7854–7860.
[7] D.T. Chao, S.J. Korsmeyer, Annu. Rev. Immunol. 16 (1998) 395–419.
[8] J.M. Adams, S. Cory, Science 281 (1998) 1322–1326.
[9] T.S. Dexheimer, D. Sun, L.H. Hurley, J. Am. Chem. Soc. 128 (2006) 5404–5415.
[10] M.I. Onyshchenko, T.I. Gaynutdinov, E.A. Englund, D.H. Appella, R.D. Neumann, I.G. Panyutin, Nucleic Acids Res. 37 (2009) 7570–7580.
[11] H. Han, L.H. Hurley, Trends Pharmacol. Sci. 21 (2000) 136–141.
[12] A.M. Burger, F. Dai, C.M. Schultes, A.P. Reszka, M.J. Moore, J.A. Double, S. Neidle, Cancer Res. 65 (2005) 1489–1496.
[13] H. Song, J.T. Kaiser, J.K. Barton, Nat. Chem. 4 (2012) 615–620.
[14] J.-T. Wang, Y. Li, J.-H. Tan, L.-N. Ji, Z.-W. Mao, Dalton Trans. 40 (2010) 564–566.
[15] L.H. Hurley, Nat. Rev. Cancer 2 (2002) 188–200.
[16] S. Neidle, G. Parkinson, Nat. Rev. Drug Discov. 1 (2002) 383–393.
[17] T.m. Ou, Y.j. Lu, J.h. Tan, Z.s. Huang, K.Y. Wong, L.q. Gu, ChemMedChem 3 (2008) 690–713.
[18] J.E. Reed, A.A. Arnal, S. Neidle, R. Vilar, J. Am. Chem. Soc. 128 (2006) 5992–5993.
[19] S. Shi, X. Geng, J. Zhao, T. Yao, C. Wang, D. Yang, L. Zheng, L. Ji, Biochimie 92 (2010) 370–377.
[20] T. Wilson, M.P. Williamson, J.A. Thomas, Org. Biomol. Chem. 8 (2010) 2617–2621.
[21] A. Ghosh, P. Das, M.R. Gill, P. Kar, M.G. Walker, J.A. Thomas, A. Das, Chem. Eur. J. 17 (2011) 2089–2098.
[22] S. Shi, J. Liu, T. Yao, X. Geng, L. Jiang, Q. Yang, L. Cheng, L. Ji, Inorg. Chem. 47 (2008) 2910–2912.
[23] D. Sun, Y. Liu, D. Liu, R. Zhang, X. Yang, J. Liu, Chem. Eur. J. 18 (2012) 4285–4295.
[24] D. Liu, Y. Liu, C. Wang, S. Shi, D. Sun, F. Gao, Q. Zhang, J. Liu, ChemPlusChem 77 (2012) 551–562.
[25] Q. Yu, Y. Liu, C. Wang, D. Sun, X. Yang, Y. Liu, J. Liu, PloS One 7 (2012) e50902.
[26] Q. Yu, Y. Liu, J. Zhang, F. Yang, D. Sun, D. Liu, Y. Zhou, J. Liu, Metallomics 5 (2013) 222–231.
[27] A. Levina, A. Mitra, P.A. Lay, Metallomics 1 (2009) 458–470.
[28] S. Satyanarayana, J.C. Dabrowiak, J.B. Chaires, Biochemistry 31 (1992) 9319–9324.
[29] M. Reichmann, S. Rice, C. Thomas, P. Doty, J. Am. Chem. Soc. 76 (1954) 3047–3053.
[30] W. Paw, R. Eisenberg, Inorg. Chem. 36 (1997) 2287–2293.
[31] J.-Z. Wu, B.-H. Ye, L. Wang, L.-N. Ji, J.-Y. Zhou, R.-H. Li, Z.-Y. Zhou, J. Chem. Soc., Dalton Trans. (1997) 1395–1402.
[32] C. Rajput, R. Rutkaite, L. Swanson, I. Haq, J.A. Thomas, Chem. Eur. J. 12 (2006) 4611–4619.
[33] J.-G. Liu, Q.-L. Zhang, X.-F. Shi, L.-N. Ji, Inorg. Chem. 40 (2001) 5045–5050.
[34] X.W. Liu, J. Li, H. Deng, K.C. Zheng, Z.W. Mao, L.N. Ji, Inorg. Chim. Acta 358 (2005) 3311–3319.
[35] M.R. Gill, J.A. Thomas, Chem. Soc. Rev. 41 (2012) 3179–3192.
[36] S.N. Georgiades, N.H. Abd Karim, K. Suntharalingam, R. Vilar, Angew. Chem. Int. Ed. 49 (2010) 4020–4034.
[37] L. Petraccone, J.O. Trent, J.B. Chaires, J. Am. Chem. Soc. 130 (2008) 16530–16532.
[38] H.-Q. Yu, D. Miyoshi, N. Sugimoto, J. Am. Chem. Soc. 128 (2006) 15461–15468.
[39] K.N. Luu, A.T. Phan, V. Kuryavyi, L. Lacroix, D.J. Patel, J. Am. Chem. Soc. 128 (2006) 9963–9970.
[40] K. Shin-ya, Telomestatin, J. Am. Chem. Soc. 123 (2001) 1262–1263.
[41] K. Paeschke, S. Juranek, T. Simonsson, A. Hempel, D. Rhodes, H.J. Lipps, Nat. Struct. Mol. Biol. 15 (2008) 598–604.
[42] K. Paeschke, T. Simonsson, J. Postberg, D. Rhodes, H.J. Lipps, Nat. Struct. Mol. Biol. 12 (2005) 847–854.
[43] D. Sun, R. Zhang, F. Yuan, D. Liu, Y. Zhou, J. Liu, Dalton Trans. 41 (2012) 1734–1741.
[44] Y. Xu, Chem. Soc. Rev. 40 (2011) 2719–2740.
[45] Y. Xu, T. Ishizuka, K. Kurabayashi, M. Komiyama, Angew. Chem. Int. Ed 48 (2009) 7833–7836.
[46] C. Zhao, J. Ren, X. Qu, Langmuir 29 (4) (2013) 1183–1191.
[47] S. Burge, G.N. Parkinson, P. Hazel, A.K. Todd, S. Neidle, Nucleic Acids Res. 34 (2006) 5402–5415.
[48] C.A. Puckett, R.J. Ernst, J.K. Barton, Dalton Trans. 39 (2010) 1159–1170.
[49] M. Van Gurp, N. Festjens, G. van Loo, X. Saelens, P. Vandenabeele, Biochem. Biophys. Res. Commun. 304 (2003) 487–497.
[50] M. Juneja, U. Vanam, S. Paranthaman, A. Bharathan, V.S. Keerthi, J.K. Reena, R. Rajaram, K.N. Rajasekharan, D. Karunagaran, Eur. J. Med. Chem. 63 (2013) 474–483.